An Approximate Electromagnetic Model for Optimizing Wireless Charging of Biomedical Implants

An Approximate Electromagnetic Model for Optimizing Wireless Charging of Biomedical Implants

Kyle van Oosterhout, Maarten Paulides, *Senior Member, IEEE*, Hans Pflug, Steven Beumer, and Rob Mestrom, *Member, IEEE*

Abstract*—*Objective: **Computational modeling is increasingly used to design charging systems for implanted medical devices. The design of these systems must often satisfy conflicting requirements, such as charging speed, specific absorption rate (SAR) and coil size. Fast electromagnetic solvers are pivotal for enabling multi-criteria optimization. In this paper, we present an analytical model based on the quasi-static approximation as a fast, yet sufficiently accurate tool for optimizing inductive charging systems.** ***Methods:*** **The approximate model was benchmarked against full-wave simulations to validate accuracy and improvement in computation time. The coupling factor of two test coils was measured for lateral and axial displacements and the SAR was measured experimentally in a PAA phantom.** ***Results:*** **The approximate model takes only 11 seconds to compute a single iteration, while the full-wave model takes 5 hours to compute the same case. The maximum difference with full-wave simulations was less than 24% and the mean difference less than 2%. Adding a novel figure of merit into the multi-criterion optimization resulted in a 16% higher charging speed. The measured results of the SAR and coupling factor are within a 5 mm coil offset margin.** ***Conclusion:*** **The proposed approximate model succeeds as a rapid prototyping tool, enabling fast and sufficiently accurate optimization for wireless charging systems.** ***Significance:*** **The approximate model is the first of its kind to compute both the coupling factor and the SAR near conducting structures fast enough to enable optimization of charging speed.**

***Index Terms*—Dosimetry, electromagnetic scattering, human exposure, inductive wireless power transfer, magneto quasi-static approximation, rechargeable implants, specific absorption rate (SAR).**

I. Introduction

ACTIVE implantable medical devices require a battery which has a limited charge capacity to power the electronics. This capacity is usually the bottleneck for the time the implant can remain in the human body and replacement requires a risky and costly surgical procedure. To reduce this dependency, a rechargeable battery can be used. For implantable devices, the implant depth can be too large for efficient capacitive charging so the most common method is inductive charging [1]. Pivotal for the efficiency of an inductive wireless power transfer system is the design of the transmitting and receiving coils. The coupling factor and quality factors of these coils, together with the load impedance, determine the charging speed of the system [2]. Furthermore, the electromagnetic fields for charging can cause undesired side effects, such as induced voltages over conductive loops in the system because of coupling with the magnetic field. Finally, strict design requirements need to be upheld to avoid heating of tissue [3], [4], which restricts charging time.

Previous works have already shown models that estimate the self-inductance, mutual-inductance and quality factor of different shapes of coils in four to six orders of magnitude less time than full-wave solvers [5], [6]. However, there are no reported models that include the electric field, SAR, or perfect electric conductors (PECs) in proximity of the coils, which are all important for wireless charging for biomedical implants.

Computing electromagnetic fields in the near-field of a current-carrying coil is a time-consuming process, especially at low frequencies. Full-wave simulations are associated with challenges in resolving electric and magnetic fields in structures or tissues that are small compared to the wavelength. Hence, the resulting linear system of equations is ill-conditioned [7]. One way to (partially) solve the aforementioned problem is by using a quasi-static approximation. For inductive charging, we assume a slowly time-varying current, which justifies using a magneto quasi-static approximation based on stationary currents. The maximum error of this approximation is roughly 15% in the specific absorption rate (SAR) [8], but the approximation decreases the computation time significantly. To improve the computation time even further in order to allow rapid prototyping and optimization, an analytic approximation of the magneto quasi-static equations can be used.

Even a very good full-wave simulation model is not fully accurate. The average difference between full-wave simulations and SAR measurements is as high as 35%, and sometimes even up to 55% [9], [10]. This is mostly due to differences in positioning due to human error, due to assumptions made in the model, or due to limitations in the simulation software. Furthermore, the

Manuscript received September 30, 2021; revised November 11, 2021; accepted November 25, 2021. Date of publication November 30, 2021; date of current version May 20, 2022. *(Corresponding author: Kyle van Oosterhout.)*

Maarten Paulides, Hans Pflug, Steven Beumer, and Rob Mestrom are with the Department of Electrical Engineering, Eindhoven University of Technology, The Netherlands.

Kyle van Oosterhout is with the Department of Electrical Engineering, Eindhoven University of Technology, 5612 AZ Eindhoven, The Netherlands (e-mail: k.v.oosterhout@tue.nl).

Digital Object Identifier 10.1109/TBME.2021.3131411

measurement equipment introduces errors, since the temperature probes, which are used to measure SAR by the power-pulse method, have an accuracy of 0.2 degrees Celsius.

In this paper, a computationally light, yet accurate magneto-quasi-static electromagnetic simulation model based on the Biot-Savart equations is proposed, which can be used to optimize an inductive wireless power transfer system for medical purposes while calculating exposure metrics according to limitations set by the ICNIRP [4]. Designing such a system is not a straightforward task. Determining and optimizing its geometrical and electrical parameters requires iterative design simulations to do quick assessment of important properties like the SAR and the coupling factor [11], [12]. In this study, we used simulations to assess the accuracy of coupling and SAR predictions to determine if this approximate model is fast and accurate enough to be used in medical applications. Hereto, we compared results against full-wave modeling in two commercial software packages (CST and Sim4Life), as indicator of the accuracy of the model, and against experimental results, to assess the accuracy of the relevant output metric, i.e. the minimum receiving current. Finally, we applied optimization with the approximate model for a realistic wireless charging use case.

II. Theory

To compute the electric and magnetic fields of an inductive wireless charging system analytically, the Biot-Savart equation can be used. An analytic solution can be found when the sources are infinitely thin finite wires with uniform current. The Biot-Savart equation to calculate the magnetic field $\mathbf{H}$ at an observation point $\mathbf{r}$ in space, caused by a current segment at source point $\mathbf{r}'$ is given by [13]

$$\mathbf{H}(\mathbf{r}) = \frac{I}{4\pi}\int_L \frac{\mathrm{d}\mathbf{l}\times(\mathbf{r}-\mathbf{r}')}{|\mathbf{r}-\mathbf{r}'|^3}, \tag{1}$$

where I is the total current through the wire, $\mathbf{l}$ is the direction of the current on point $\mathbf{r}'$ on the current-carrying line segment L.

If the current is not stationary, but varies slowly, harmonically in time as $I(t) = Ie^{j\omega t}$, where ω is the angular frequency of the variation, the electric field can be found by computing the magnetic vector potential $\mathbf{A}$, which, for the same infinitely thin wire carrying a uniform current, equals

$$\mathbf{A}(\mathbf{r}) = \frac{I\mu_0}{4\pi}\int_L \frac{\mathrm{d}\mathbf{l}}{|\mathbf{r}-\mathbf{r}'|}, \tag{2}$$

where μ_0 is the free space permeability. Once the magnetic vector potential is known, the electric field can be calculated using

$$\mathbf{E}(\mathbf{r},t) = -\mathrm{j}\omega\mathbf{A}(\mathbf{r})e^{-\mathrm{j}\omega t}. \tag{3}$$

It can be noticed that the electric field is time-dependent, whereas the magnetic field is not. This is due to the magneto quasi-static approach that has been used, which assumes that the magnetic field may be considered stationary. The approximation of the magnetic field will therefore be equal to

$$\mathbf{H}(\mathbf{r},t) = \mathbf{H}(\mathbf{r})e^{-\mathrm{j}\omega t}. \tag{4}$$

To check the validity of this assumption, we determine to what extent Maxwell's equations are still satisfied. For this purpose, the magnetic field is computed numerically using the curl of the electric field, according to Faraday's law:

$$\mathbf{H} = -\frac{\nabla\times\mathbf{E}}{j\omega\mu}. \tag{5}$$

By computing the magnetic field in this way using Matlab and comparing the solution to the analytic expression (1), the discrepancy between the two magnetic fields can be found to be on average 0.01% and maximally 1%, on a finite mesh.

Coils of arbitrary shapes can be constructed with a (large) amount of finite straight line segments. Superposition then allows for the calculation of the electromagnetic fields for the collection of line segments. The computation time, however, scales linearly with the number of line segments.

In the approximate model described above, it is assumed that there are no strongly conducting materials near the location where the field is computed. However, this is not a realistic situation, because most implanted electronics are protected with a titanium cover. Because titanium is much more conductive than the dielectrics considered in the body, it can be approximated as a perfect electric conductor (PEC). For both the electric and the magnetic field, the effects of the PEC can be computed analytically under the assumption that the field is homogeneous. This assumption naturally does not hold for the fields induced by a coil. The magnetic field, however, can be approximated as locally homogeneous for positions further than 5 mm away from the coil, as is shown by inspection of a typical simulated field. In this case, analytical results can still be used to investigate the effect of fields on perfect electric conductors in the region of interest.

When a perfect electric conductor is present in a (homogeneous) magnetic field, a current density is induced on the outside of the conductor for which the magnetic field can be calculated using the magnetic scalar potential [14]

$$\mathbf{H} = -\nabla\Psi, \tag{6}$$

where $\mathbf{H}$ is the total magnetic field and Ψ is the scalar potential.

Computing this for spherical PECs in a locally homogeneous field can be done analytically using the Laplace equation in spherical coordinates. The perturbation of the magnetic field due to the perfect electric conductor is found to be equal to the magnetic field of a dipole in the center of the sphere:

$$\mathbf{H}(r) = \frac{3\hat{\mathbf{r}}(\mathbf{m}\cdot\hat{\mathbf{r}})-\mathbf{m}}{4\pi r^3}, \tag{7}$$

where $\hat{\mathbf{r}}$ is the unit vector in the direction of $\mathbf{r}$, and $\mathbf{m}$ is the magnetic dipole moment, which is equal to $-2\pi H_0 r^3\hat{m}$, and $\hat{m}$ is the direction of the dipole, or in this case, the direction of the magnetic field.

As a result of the magneto quasi-static approach, the vector potential of the magnetic dipole derived for the PEC sphere in a homogeneous magnetic field can also be converted into the change in the electric field due to the presence of the PEC sphere, because the perturbation of the magnetic field is modeled as a magnetic dipole too. The vector potential of a magnetic dipole

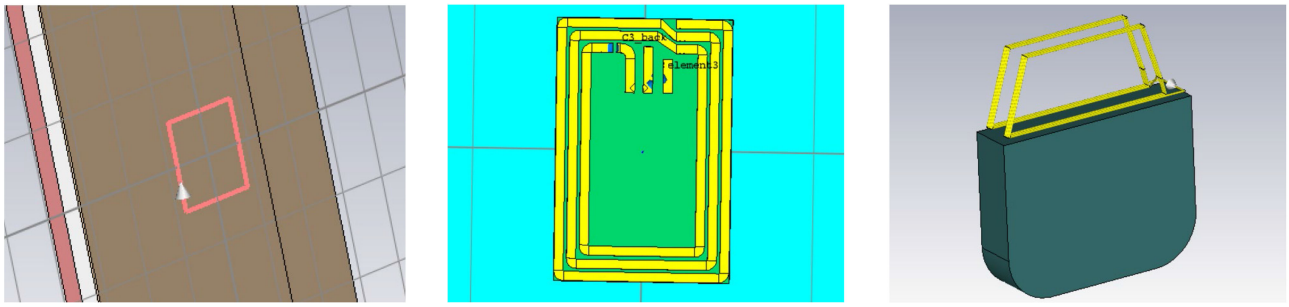

(a) Infinitely thin loop modelled in CST (image with angle to show layers)

(b) TXcoil modelled in CST in same position as in image (b)

(c) IPG modelled in CST

Fig. 1. Overview of CST models.

is [15]

$$\mathbf{A}(\mathbf{r}) = \frac{\mu}{4\pi}\frac{\mathbf{m}\times\mathbf{r}}{r^3}, \tag{8}$$

which can easily be computed numerically. Using superposition with the vector potential computed from the current through the coil (2), the total electric field can be found.

III. Methods

The first requirement to be set is the maximum error introduced by the model. As stated in the introduction, the reported minimum measurement error compared to a full-wave simulation for the SAR is 35%, and sometimes even up to 55% [9], [10]. Therefore, in order to not make the error introduced by the model dominant, the maximum deviation between this model and numerical methods has to be below 35%. The second requirement is the computation time. The second requirement is the computation time of the model. Typically, a magneto quasi-static approximation is about one order of magnitude faster than its full-wave equivalent, which could take a simulation time from 10 to 15 minutes or longer. This is too slow for iterative optimization, since many function evaluations (i.e. simulations) need to take place. Furthermore, a wireless power transfer system can have many variables to be optimized, relating, for instance, to the geometry of the transmitting coil, the geometry of the receiving coil, and the charging current. To be viable for rapid design iteration, the approximate model should allow for a full optimization of such a realistic case (with a three-dimensional parameter space) within a reasonable amount of time, say 24 hours.

A. Field Predictions vs Full Wave Modeling

To test the fields calculated by the approximate model against the requirements, similar but much more detailed models were simulated in both CST Studio Suite [16] and Sim4Life [17]. These models consists either of a single transmit coil, or a combination of a transmit and receive coil. Two different transmitting coils were implemented. The first one is an infinitely thin rectangular coil of 7.16 cm by 5.74 cm (see Fig. 1(a)), and the second one is a rectangular coil with three spiraling turns on both the front and the back side of an FR4 PCB with the same size as the infinitely thin rectangular coil (see Fig. 1(b)). This PCB coil will be referred to as the TXcoil. Both models were designed in CST and imported into Sim4Life. The Implantable Pulse Generator (IPG) consists of a receiving coil of trapezoidal shape with a lower base of 3.8 cm and an upper base of 2.8 cm and a height of 1.6 cm, on top of a perfect electric conductor casing in the form of a box of 4.5 cm (x-direction) by 3.5 cm (y-direction), and a depth of 1 cm (Fig. 1(c)). Finally, to assess the effect on human tissue, the body was modeled as a layered structure stack of 1.3 mm skin, 1 cm fat, and 1 cm muscle. This is assumed to be representative for the treated population [18]. The transmitting coil was positioned 5 mm from the skin, which is a realistic thickness of a casing for the transmitting coil. The casing of the transmitting coil is not taken into account in the simulations explicitly because of the magneto-quasi static model. The receiving coil was positioned on the fat-muscle interface.

Simulations with the approximate model were done in MATLAB 2019b. Full wave simulations were performed on the same laptop (Intel(R) Core(TM) I7-9750H CPU, NVIDIA GeForce GTX 1650 GPU) using the frequency domain method of CST Studio Suite and the time domain method of Sim4Life. In the low frequency finite element method (FEM) simulations in CST, adaptive mesh refinement was used to ensure a sufficiently detailed mesh, with a maximum of 1 million mesh cells to stay within the available memory. Furthermore, a perfectly matched layer box of 12 cm around the simulation domain was added in every direction to minimize the effect of boundary conditions on the fields. In Sim4Life, a finite difference time domain (FDTD) simulation was performed over 15 oscillation periods to obtain a steady state solution. An initialization of 1 period was used. The boundaries of the domain of simulation were set to absorbing boundary conditions. In addition, in both CST and Sim4Life, magneto quasi-static simulations based on FEM were performed as well to inspect the error introduced due to the magneto-static approximation. The errors were determined throughout slices in the same orientation as the two-dimensional coil ($x-y$) by computing the error relative to the maximum absolute value of the full-wave solution in the slice, because taking the local percentual error gives large errors at very low field values because of small numerical inaccuracies, which are not relevant to this study. The maximum of the relative errors in all slices is the total maximum error.

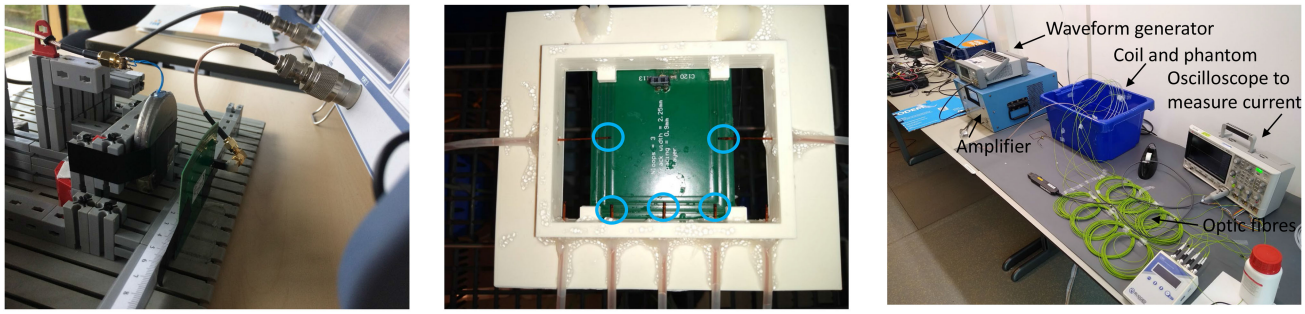

(a) Overview of coupling factor measurement setup

(b) Close-up of Txcoil and temperature probe positions (inside the blue circles)

(c) Overview of SAR measurement setup

Fig. 2. Overview of measurement setup.

B. Coupling Factor vs Measurements

The behaviour of the coupling factor was measured by fixing the TXcoil in a certain position and by scanning the receiving coil over it, at a fixed distance (z-position) of 3 cm and a range for x and y from 0 to 10 cm. The positioning tolerance was a few millimeters. Alternatively, the x and y-direction were fixed to 0 cm and the z-direction was varied between 0 and 7 cm. A network analyzer was used to measure and compute the inductances of both coils as well as the mutual inductance between them. With these values, the coupling factor k can be computed as:

$$k = \frac{M_{12}}{\sqrt{L_1 L_2}}, \tag{9}$$

where M_{12} is the mutual inductance between the two coils, L_1 is the self inductance of the primary coil and L_2 is the self inductance of the secondary coil. The total setup can be seen in Fig. 2(a).

C. Specific Absorption Rate vs Measurements

The SAR was measured by performing an experiment with a polyacrylic acid (PAA) phantom, made according to the ISO 10974:2018 [19] standard for making a 1.2 S/m phantom at approximately 64 MHz, with a DC conductivity of 1.03 S/m. This was measured with a HANNA HI991301 EC meter. The phantom has similar properties to human fat, except for the electrical conductivity which has been boosted 25 times to be able to measure the change in temperature. The setup for the SAR measurements consisted of the TXcoil, tuned to resonate at 6.78 MHz, through which a current of 3 A peak to peak was induced with a signal generator at the same frequency and an RF amplifier. Rugged L201 fiber optic temperature probes were then used to measure the temperature in the phantom, which were positioned as seen in Fig. 2(b). The probes at the bottom side of the image were placed 15 mm apart. One additional probe was placed in the corner of the phantom to measure the background temperature.

Just after the start of a measurement, no temperature diffusion is taking place yet. Therefore, the SAR can be related to the time derivative of temperature at the start of the heating process [20] by simplifying the Pennes-Bioheat equation to:

$$\mathrm{SAR} = c\frac{dT}{dt}, \tag{10}$$

where c is the specific heat of the material and T is the temperature. To decrease the effect of noise, an exponential fit was made over the complete temperature measurement and the derivative of this fit was used.

To obtain accurate results, no current was run through the coil in the first 15 minutes of every experiment to test the stability of the steady state temperature and to start from room temperature. Next, the current was switched on for 40 minutes to heat the phantom. After the current was switched off, 40 minutes of time was used to allow the phantom to cool down to room temperature again. This experiment was repeated three times and the temperature measurements are averaged over the three experiments. The total setup is shown in Fig. 2(c).

D. Optimization of the Go-2 System

To show how the derived approximate model can be applied to a realistic case, the optimization of the Go-2 system of GTX medical [21] is used as an example. The Go-2 system is designed to stimulate the neurons in the spinal cord of patients with a spinal cord injury in order to invoke a response that allows the patient to move their previously paralyzed legs again [22]. To do this, a so-called motion controller (MC) is programmed to send tasks to an implantable pulse generator (IPG), which stimulates a desired region on the spinal cord with the adequate signal. The TXcoil to charge the battery of the IPG is located in the motion controller. The IPG itself is implanted in the abdomen.

The Go-2 system has several constraints that have to be taken into account when optimizing the system:

- The SAR averaged over 10 grams cannot exceed 2 W/kg anywhere inside the body [4].
- The system has to charge as fast as possible for implantation depths between 1 cm and 5 cm, where the implantation depth is defined as the distance from the transmitting coil to the middle of the IPG.

To make sure the SAR constraint is met, the maximum simulated SAR had to be below 1.5 W/kg, allowing for some safety margin, due to the 25 % maximum error of the model, which will be explained in Section IV. Keeping the SAR below a maximum

of 2 W/kg ensures no harm will be done to human tissues due to the heating effect of the charging [23], [24]. Additionally, the measurements have been done with a phantom that mimics human tissues without perfusion, and thus the heating in living tissue will be limited even more.

Furthermore, a clear figure of merit had to be introduced to determine when the system is optimal. The two most important variables for charging speed are the input current (current inserted into the transmitting coil), which is linearly related to the charging speed, and the coupling factor k, which is related to the charging efficiency defined as

$$\eta = \frac{k^2 Q_s Q_r}{(1 + k^2 Q_s Q_r \frac{\alpha}{\alpha+1})} \frac{\alpha}{(\alpha+1)^2}. \tag{11}$$

Here η is the charging efficiency between the two coils, Q_s is the quality factor of the transmitting coil, Q_r is the quality factor of the receiving coil and α is the load factor [2]. For the Go-2 system, the quality factor of the receiving coil is calculated to be approximately 35 and the load factor is approximately 0.13. The quality factor of the transmitter coil depends on the shape of the coil, and is computed by assuming the resistance of the coil is linearly related to the total length of current carrying lines and according to

$$Q_s = \frac{2\pi f L}{R}, \tag{12}$$

where f is the charging frequency (6.78 MHz), L is the numerically computed inductance of the transmitter coil, and R is the resistance of the transmitter coil. The figure of merit is the total minimum receiving current I_r, which is the minimum current induced in the receive coil for the given distances. This can be expressed as

$$I_r = I\eta, \tag{13}$$

where I is the maximum current for which the SAR is less than or equal to 1.5 W/kg and η is given in (11). The variables that were included in the optimization are the length and width of the transmitting coil and the charging current.

An important part of the optimization of a wireless charging system is the coupling of the magnetic field into electronics or wires, leading to unintentional stimulation. In this case study, this might occur because of loops in the cable between the receiving coil and the stimulation electrodes (lead cable), which in turn introduces an increased SAR in the body. It is common for the surgeon to make a loop behind the IPG with the lead cable during the implantation of the IPG and the lead. This is because the lead lengths between IPG and electrodes are standardized, and thus often the lead is too long, requiring a loop to reduce the effective length. Since inductive charging is used, loops in cables could pick up magnetic flux. This could induce a current that stimulates the neurons in the spine, or induce a SAR higher than the limit due to the fact that the currents travelling through the body induce fields.

Using the approximate model, the magnetic flux that goes through the loop can be calculated when the geometry and position of the loop is known. A surgeon usually makes the conducting loop about the size of the IPG (around 5 cm diameter) behind the IPG. For a worst case scenario analysis, the distance between the loop and the transmitting coil is therefore taken to be 15 mm, with an IPG casing of 10 mm thickness and the transmitting coil 5 mm from the skin.

To quantify the impedance between several positions inside the human body, which is necessary to compute the SAR from a given current coupling in the lead wire, a simulation model study has been performed. To obtain an estimate of the maximum current density and SAR through the body due to unintentional stimulation, the Sim4Life ViP models Duke and Fats were used [25]. In the simulations, the SAR and current density for multiple voltages over the lead wire were determined. The results show a linear trend for the current density versus voltage, and a quadratic trend for the SAR versus the voltage. Linear and quadratic fits were made to these curves, respectively, to compare with simulations with the approximate model at any voltage.

Given the aforementioned requirements and by using the figure of merit, the Go-2 system was optimized for optimal transmitting coil size by sweeping over 9 sizes in x-direction (linear from 15 mm to 139 mm) and 9 sizes in y-direction (linear from 10 mm to 93 mm) by keeping the same amount of simulation lines and increasing their lengths linearly to increase the length or width.

IV. Results

In this section, first a comparison is made between the approximate model and commercial simulation software packages CST Studio Suite and Sim4Life for the infinitely thin loop and the TXcoil. Next, the calculations of the coupling factor between the TXcoil and the coil of the IPG are validated by comparing them to measurements at different positions and distances. Finally the SAR is determined from the electric field and compared to the temperature measurements.

A. Comparison Approximate Model With CST and Sim4Life

In Fig. 3 the magnitude of the electric and magnetic field can be seen of the TXcoil in a single observation slice (at $z = 10$ mm from the coil) for the approximate model and the CST solution together with the relative error between the two. The figures show that the magnetic field error is mostly below 10%, except just above the current source in CST, where the results differ because the Biot-Savart equation does not take reflections within the source into account that occur because the source is not perfectly matched in CST. These results of the electric field are very similar to the ones of the magnetic field, with a 20% error above the current source, and a maximum of 11% elsewhere. The maximum errors between the quasi-static model, CST and Sim4Life have also been calculated over the simulated tissue. These values and the computation times are listed in Table I. Most results of the approximate model in the table are compared to the electromagnetic fields from CST and Sim4Life averaged, except for the values with a "*," which were only simulated in CST.

Several different cases are compared. The "(MQS)" tag indicates that the commercial solver results are computed with the

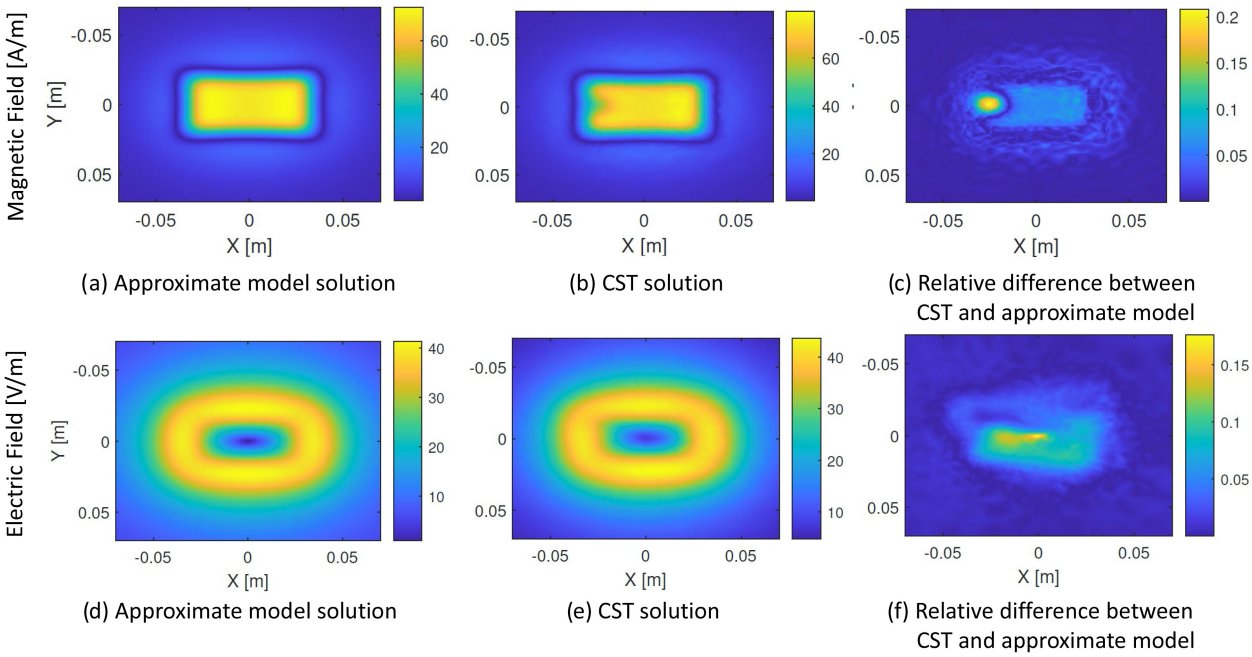

Fig. 3. Magnetic field component H_z in A/m and Electric field magnitude in V/m computed by the approximate model (a, d), The results of the CST simulation for the same fields (b, e) as well as the relative error between the approximate and CST solutions (c, f), computed at a z-slice 10 mm from the coil.

TABLE I
COMPUTATION TIMES AND ERROR OF THE ABSOLUTE VALUE OF THE FIELD COMPONENTS IN THE APPROXIMATE MODEL COMPARED TO THE AVERAGE BETWEEN CST AND SIM4LIFE FOR ALL CASES CONSIDERED. THE VALUES WITH A "*" HAVE ONLY BEEN COMPARED TO CST

Case [CST Tetrahedrons]	Time full-wave [s]	Time analytic [s]	Avg Speed improvement	Max deviation E	Mean deviation E	Max deviation H	Mean deviation H
Single infinitely thin loop [9.26e5] (MQS)	1400	2.3	$\sim$ 600	1.2%*	0.3%*	2.2%	0.1%
Single infinitely thin loop [9.26e5]	3.1e4	2.3	$\sim$ 14000	3.3%	0.5%	5.8%	0.1%
Single infinitely thin loop + PEC Sphere [9.27e5]	3.1e4	6.7	$\sim$ 4600	9.8%	0.5%	17.4%	0.3%
Single infinitely thin loop + PEC Box [9.27e5]	5.4e4*	43.5	$\sim$ 1200*	19.9%*	0.3%*	18.1%*	1.4%*
Realistic TXcoil - no field above input [4.63e5] (MQS)	500	7.7	$\sim$ 65	6.3%*	1.3%*	10.1%*	2.0%*
Realistic TXcoil - no field above input [4.63e5]	4.6e4	7.7	$\sim$ 6000	11.7%	1.9%	11.5%	1.6%
Realistic TXcoil + PEC Box [8.64e5]	6.1e5	54	$\sim$ 110000	23.3%*	1.8%*	20.1%*	0.7%*
Maximum deviations	-	-	-	**23.3%**	**1.9%**	**20.1%**	**2.0%**

magneto quasi-static solver, the "+ PEC Sphere" tag indicates that a 5 mm radius PEC sphere is modelled in the center of the current loop at 2 cm distance. The "+ PEC Box" tag indicates that a 4.5 cm by 3.5 cm by 1 cm PEC box has been modelled to mimick the effect of the IPG. For the approximate model, this has been done by placing $11 \times 8 \times 3$ PEC spheres of 0.3 cm radius in the shape of the box at 2 cm distance from the current loop which has roughly the same dimensions as the titanium IPG casing. The amount of spheres have been chosen by making a trade-off between accuracy, computational speed and memory costs. When calculating the accuracy of the PEC box, the first 2 mm around the box has not been taken into account as the spheres inherently overestimate the fields very close to the box because of the lack of PEC at the whole boundary.

CST computes both the electric and magnetic field at the same time, and therefore the computation time can only be compared by taking the sum of the computation time of the electric field and the magnetic field using the approximate model and comparing it with the time CST takes to compute the fields.

From the deviation results in Table I, it can be seen that for the single infinitely thin loop, the maximum deviation in the fields is 6%. When comparing the results with a TXcoil of finite thickness, the maximum deviation becomes much larger, namely 32.6%. Further inspection shows that this deviation is almost exclusively directly above the current source in CST. By excluding this part from the results a maximum deviation of 11.5% is obtained, which corresponds to the previously reported deviation at 10 mm distance (Fig. 3(c) and (f)). Adding

TABLE II
EXAMPLE COMPUTATION TIMES OF THE INFINITELY THIN WIRE MODEL ON CST AND THE APPROXIMATE MODEL FOR VARYING MESH GRIDS

	Domain x [m]	Domain y [m]	Domain z [m]	Amount of cells	Computation Time [s]	Speed up w.r.t. CST
CST	0.401	0.451	0.278	9.26e5	1.8e4	1
Similar approximate model	0.401	0.451	0.278	9.33e5	3.25	5.5e3
Fine approximate model	0.281	0.331	0.158	2.8e7	11.3	1.6e3

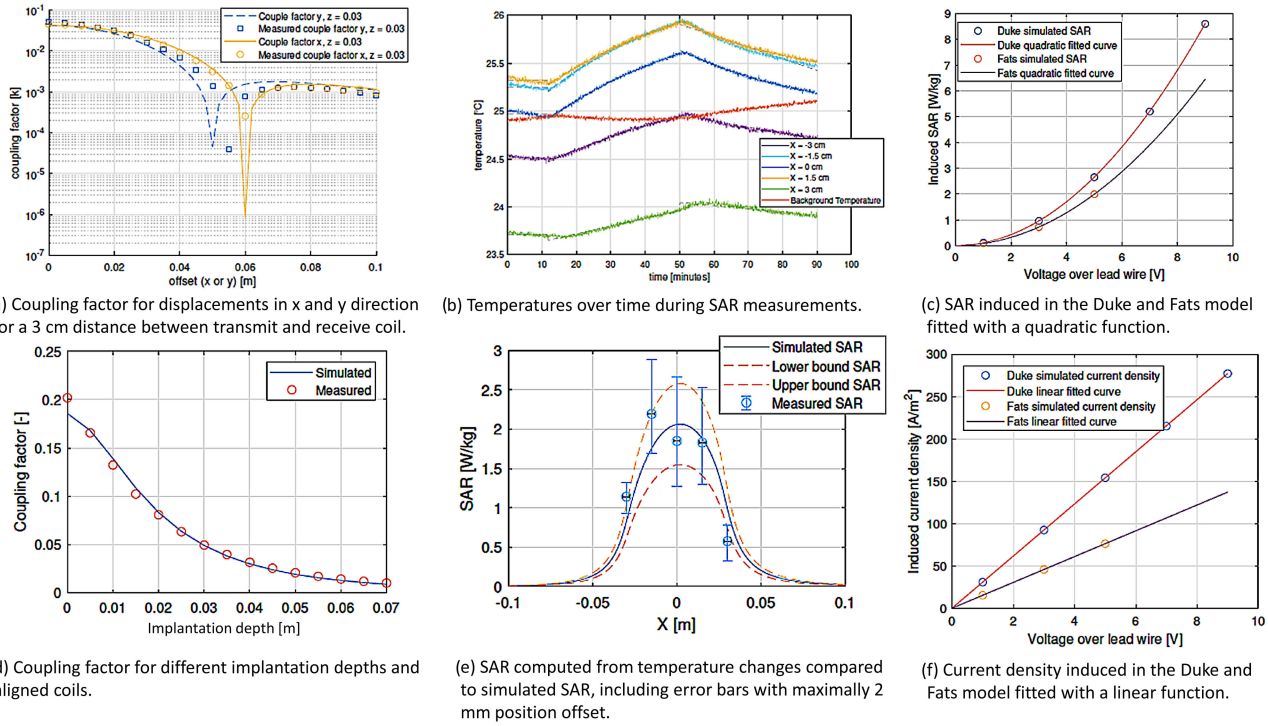

(a) Coupling factor for displacements in x and y direction for a 3 cm distance between transmit and receive coil.

(b) Temperatures over time during SAR measurements.

(c) SAR induced in the Duke and Fats model fitted with a quadratic function.

(d) Coupling factor for different implantation depths and aligned coils.

(e) SAR computed from temperature changes compared to simulated SAR, including error bars with maximally 2 mm position offset.

(f) Current density induced in the Duke and Fats model fitted with a linear function.

Fig. 4. Results of the coupling factor measurements and simulations (a, d), the SAR measurments and simulations (b, e) and the Sim4Life simulations in the Duke and Fats model for different induced leadwire voltages (c, f).

a perfect electric conductor increases the deviation further, up to a maximum of 23%.

To further benchmark the computation times of the approximate model, the single, infinitely thin loop has been used to find the speed increase. These results are listed in Table II. CST takes 18000 seconds to compute, while the same amount of cells take only 3.25 seconds to compute with the approximate model. However, these results are calculated using a step-size of 3.8 mm in every direction, which is too large to be useful in the application of wireless charging in the human body. Furthermore, because boundary conditions are not needed in the analytical method, the volume that needs to be calculated can be reduced by roughly 12 cm in every direction. With a reduced step size of 0.8 mm, the finely sampled approximate model takes 11.3 seconds to compute which is still 1600 times faster than CST.

The suitability of the approximate model for computating the electromagnetic fields and SAR is validated by the comparison of the two state-of-the-art commercial modelling tools (CST and Sim4Life). Fig. 5 shows very similar deviations between the three methods.

Finally, since the approximate model is based on quasi-static considerations, based on a stationarity assumption of the current through the loop, it is useful to determine the applicability range for the approximate model in terms of operation frequencies. For this purpose, the full-wave results for the TXcoil were compared to the approximate model results at different frequencies. These results are shown in Fig. 6. Starting at frequencies from about 10 MHz, the error starts increasing, making the model not useful for devices with frequencies higher than approximately 15 MHz.

B. Comparison Coupling Factor With Experimental Measurements

Using the mutual and self inductances of the TXcoil and the receiving coil, which can be found either analytically [5] or numerically as the magnetic field of the primary coil is already computed, the coupling factor can be found with Eq. (9). To avoid the singularity that occurs when the source and observation point are coincident, the total magnetic field with a positive z-component on the z-slice 2 mm from the coil is used. To validate the calculation of the coupling factor, the coils are measured in a test setup to find the coupling factor between the transmitting coil and the receiving coil, which are then compared to the numerically simulated coupling factor with the approximate model. The results for the two sets of measurements as described in Section III are depicted in Fig. 4(a) and (d).

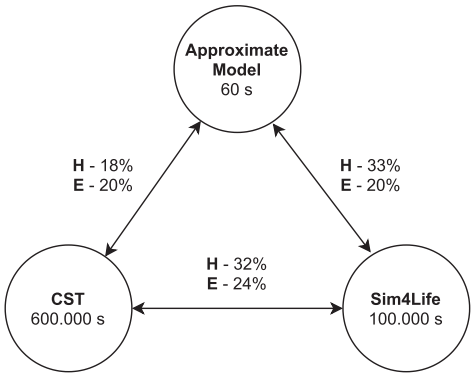

Fig. 5. Comparison of the deviation (maximum difference relative to the maximum field value) and approximate computation time of CST, Sim4Life and the approximate model.

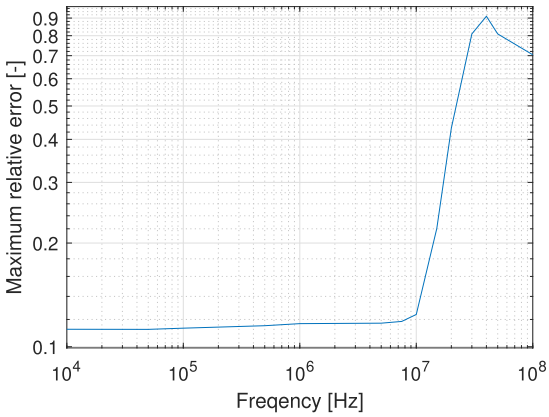

Fig. 6. Maximum relative error in the magnetic field of the approximate model for different frequencies.

From Fig. 4(d). It can be observed that the difference between measurements and simulations for the x-direction are small enough to claim that the approximate model accurately describes reality, but in the y-direction there is an offset of approximately 5 mm. This is most likely a positioning error in the measurement setup because it is difficult to exactly place the receiving coil and the transmitting coil aligned to millimeter precision. Fig. 4(a) shows the aligned coupling factor at variable z distance. The differences between measurement and simulation is minimal, except at 0 mm. This error occurs because the receiving coil is at the singularity of the transmitting coil, which occurs when trying to compute fields close to the current path due to the singularity in the Biot-Savart equations.

C. Comparison Specific Absorption Rate With Experimental Measurements

An example of the temperatures measured with the described method is shown in Fig. 4(b). From the temperature trends, the SAR is computed as detailed in Section III-C. The SAR is computed for five points under the coil wire furthest from the tuning capacitors in order to minimize interference from the source driving the coil. The probes have been placed above the coil because the temperature change will be highest closer to the coil. The five measurement points are at the center of the short side of the coil, the two points 15 mm from the center, and the two points 30 mm from the center. The result of these measurements can be seen in Fig. 4(e). In Fig. 4(b), the average temperature over time is shown. The temperatures correlate well with the exponential functions, which are the expected solutions to the Bioheat equation. The placements of the temperature probes had to be done by hand, thus a deviation of maximally 2 mm is expected. The upper and the lower bound are the maximum and minimum simulated SAR within 2 mm of the expected position. From these results it can be seen that the measured SAR is indeed below the 35 to 55% error [9].

D. Case Study: Optimization of the Go-2 System

The results of the Sim4Life simulations to find the maximum SAR and current density can be seen in Fig. 4(c) and (f). The Duke model is found to be the worst case scenario because its effective impedance (induced voltage needed between lead and IPG to get a total current of 1 A through the body) of 110 Ω is much smaller than that of the Fats model (340 Ω). Therefore the results of Duke are used in the optimization.

The results for optimizing the Go-2 system are shown in Fig. 7. These results confirm the expectation that a bigger coil will increase the minimum coupling factor, but it will also increase the maximum SAR. The chosen figure of merit finds an optimum for a coil of 7.7 cm by 8.3 cm, yielding a minimum coupling factor of $k = 0.018$, a maximum coupling factor of $k = 0.102$ and a maximum transmitting current of 1.08 A, which would give a minimum receiving current of 0.27 A. Computing the results for the complete sweep of 162 points takes approximately 2.5 hours, which is almost half the time it would take the full-wave solver in CST to compute *a single data point*. The optimization progress could be sped up even further by using an optimization algorithm rather than a sweep.

A common optimization method in practice is to get the highest possible coupling factor within the given constraints. By deriving a new practical figure of merit that is more relevant to the final charging speed of an implantable pulse generator and using the approximate model to optimize for this figure of merit, a higher charging speed can be obtained.

For the Go-2 system the coil with the optimal coupling factor is 13.9 by 7.2 cm. This will give a minimum coupling factor of 0.021, rather than the 0.018 given by the approximate model. The maximum current to remain below the SAR limits are, however, 0.71 and 1.08 A respectively, meaning that even though maximizing the coupling factor gives a higher charging efficiency, it results in a lower charging current of 0.23 A, which is only 86% of the optimal current (0.27 A). This therefore means that using the fast approximate model increases the maximum current that can be received in the IPG, and therefore the charging time by 16%.

V. Discussion

The results of the previous section show that the maximum deviation of the model compared to the full-wave solutions is less than 25%, and the average deviation is only 2%. Furthermore, the measured coupling factor is predicted well, taking positioning

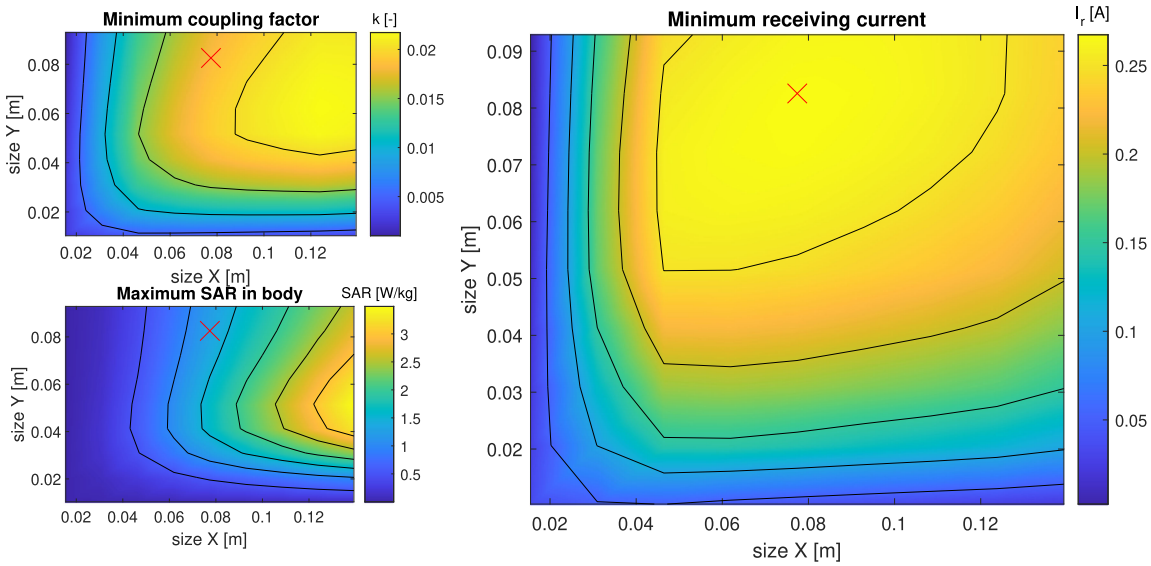

Fig. 7. Results of the approximate model sweeping over the size of the transmitting coil. The contour lines are at the numbers on the colorbar. The cross is point with the highest minimum receiving current.

errors (5 mm) into account. The SAR also agrees mostly, within 2 mm sensor position deviation. Therefore, considering that both the measured coupling factor and heating of the SAR are within the expected values of the approximate model, and observing that the deviation between Sim4Life and CST is even bigger than the deviation between CST and the approximate model, it can be concluded that the approximate model does not under-perform compared to CST or Sim4Life.

To elaborate on this result, all deviations in the electric field are below 11%, except at locations where a PEC structure is introduced. The error in the point SAR is proportional to the squared error of the electric field, and thus the maximum error in the point SAR is below 23%. An averaging technique that would induce no further error would enable to lower this to around 15% Laakso *et al.* [8] found as the inherent error of the magneto quasi-static approximation at 11.36 MHz. This shows that the other approximations made for the model induce an error of about than 4%, which is again in line with the 5.1% error compared to the extra error in the full-wave magneto quasi-static solver.

Furthermore, because all measurement setups were built by hand, a certain offset can be expected due to the inability to position the coils and the measurement probes within millimeter accuracy. Taking into account an offset of maximally 5 mm, all coupling factor measurements and simulations agree with a maximum deviation of 25%, for coil off-sets up to 5 mm, see Fig. 4(a). This proves that the coupling factor can be accurately predicted by the model. With the same reasoning, a shift of 2 mm can make the deviation between measured SAR and the model less than 35%, showing that the model achieves similar accuracy as full-wave solutions.

Comparing the approximate model to literature discussing models for fast computation of coupling factors between coils, it can be seen that the approximate model is slower by two to three orders of magnitude than an analytical model achieving similar accuracy compared to full-wave solvers as well as measurements [6], and slightly slower compared to a model achieving better accuracy [5]. The advantages of the approximate model compared to those models are firstly the addition of the electric field to the model, which allows for computation of the SAR, which is indispensable for any inductive charging in the proximity of humans or animals. Secondly, the approximate model also proposes a method of adding PEC structures, which will always be present in biomedical implants in the form of an IPG.

There are, however, multiple limitations to the technique described. Firstly, the approximate model is based on coils constructed from infinitesimally thin line segments, which excludes charged objects and magnetizable materials such as ferrite, which are normally used on the transmitting side. Another limitation is the magneto quasi-static assumption of the solution, limiting the applicability of the model to frequencies below 15 MHz. Finally, the addition of perfect electric conductors increases the error in the fields significantly up to 23%, which is due to the limited amount of PEC spheres that can be used because of the large memory cost of computing the field displacement. To improve the accuracy without increasing the computation time, further research can be done on analytical solutions for the interaction of homogeneous magnetic fields on PEC objects of various (non-spherical) shapes.

Despite the limitations, the approximate model's computational cost reduction of a factor 1600 gives it the opportunity to be used as a rapid prototyping tool. It can generate a fast indication of the SAR and coupling factor of the system, allowing for optimization of multiple parameters. The result of this optimization is about 16% better than trying to maximize the efficiency experimentally. A validation with a realistically modeled PEC casing could then follow for only the optimal case(s) to verify the found results with a generally accepted simulation tool. At the end of the design stage, it is recommended to also perform experimental verification.

VI. Conclusion

To conclude, the approximate model is able to compute the electric and magnetic fields of an inductive power transfer system within the 35% expected error when accounted for positioning errors in the measurements. Comparing the model to conventional full-wave solvers gives a maximum deviation of 23%, and an average one of less than 2%. Furthermore, the approximate model takes only 2.5 hours to compute 162 realistic data points, which is on average less than a minute of computation time per data point. A single data point computed in CST would take two times as long as the complete optimization. After the optimization there is the possibility to do a verification simulation with a full-wave solver such as CST or Sim4Life or experimental verification. These results confirm that the approximate model indeed succeeds as a rapid prototyping tool, which enables fast and sufficiently accurate optimization for inductive wireless charging systems. Thus, The approximate model is the first of its kind to compute both the coupling factor and the SAR in proximity of perfect electric conductor structures fast enough to allow for optimization of charging speed. This can potentially speed up the design process of biomedical wireless charging systems significantly as well as improve the achievable charging speed within SAR limitations.

References

[1] J. Dai and D. C. Ludois, "A survey of wireless power transfer and a critical comparison of inductive and capacitive coupling for small gap applications," *IEEE Trans. Power Electron.*, vol. 30, no. 11, pp. 6017–6029, Nov. 2015.

[2] M. Etemadrezaei, *22 – Wireless Power Transfer*, M. H. B. T. P. E. H. F. E. Rashid, Ed. Butterworth-Heinemann, 2018, pp. 711–722. [Online]. Available: http://www.sciencedirect.com/science/article/pii/B9780128114070000246

[3] A. Christ *et al.*, "Assessing human exposure to electromagnetic fields from wireless power transmission systems," *Proc. IEEE*, vol. 101, no. 6, pp. 1482–1493, Jun. 2013.

[4] International Commission on Non-Ionizing Radiation Protection (ICNIRP), "International commission on non-ionizing radiation protection (ICNIRP) guidelines for limiting exposure to time-varying electric, Magnetic and Electromagnetic Fields (up to 300 GHz "), *Health Phys.*, vol. 74, no. 4, Apr. 1998.

[5] S. Babic *et al.*, "Mutual inductance calculation between circular filaments arbitrarily positioned in space: Alternative to Grover's formula," *IEEE Trans. Magn.*, vol. 46, no. 9, pp. 3591–3600, Sep. 2010.

[6] S. Raju *et al.*, "Modeling of mutual coupling between planar inductors in wireless power applications," *IEEE Trans. Power Electron.*, vol. 29, no. 1, pp. 481–490, Jan. 2014.

[7] S.-H. Lee and J.-M. Jin, "Application of the tree-cotree splitting for improving matrix conditioning in the full-wave finite-element analysis of high-speed circuits," *Microw. Opt. Technol. Lett.*, vol. 56, no. 3, pp. 748–753, 2008.

[8] I. Laakso *et al.*, "Quasistatic approximation for exposure assessment of wireless power transfer," *IEICE Trans. Commun.*, vol. E98B, no. 7, pp. 1156–1163, 2015.

[9] B. B. Beard *et al.*, "Comparisons of computed mobile phone induced SAR in the SAM phantom to that in anatomically correct models of the human head," *IEEE Trans. Electromagn. Compat.*, vol. 48, no. 2, pp. 397–407, May 2006.

[10] I. Laakso *et al.*, "Evaluation of SAR in a human body model due to wireless power transmission in the 10 MHz band," *Phys. Med. Biol.*, vol. 57, no. 15, pp. 4991–5002, 2012.

[11] Y. Aoki *et al.*, "Calculation of coupling factor for kHz-band wireless power transfer system using numerical human models," *Proc. Int. Workshop Electromagnetics: Appl. Student Innov. Competition*, 2015, pp. 1–2.

[12] S. Mutashar *et al.*, "Analysis and optimization of spiral circular inductive coupling link for bio-implanted applications on air and within human tissue," *Sensors*, vol. 14, no. 7, 2014, pp. 11522–11541,.

[13] W. H. Hayt and J. A. Buck, *Engineering Electromagnetics*, 8th ed. London, U.K: Mcgraw Hill Higher Education, pp. 180–187, 2012.

[14] H. A. Haus and J. R. Melcher, "Electromagnetic fields and energy," in *Electromagnetic Fields and Energy*. Englewood Cliffs, NJ, USA: Prentice-Hall, *ch. 8.4*, 1989.

[15] T. Chow, "Electromagnetic theory: A modern perspective," in *Electromagnetic Theory: A Modern Perspective*. S. Weaver *et al.*, Eds. Burlington, Massachusetts, USA: Jones and Bertlett Publishers, Inc., *ch. Magnetosta*, 2006, pp. 146–150.

[16] CST GmbH, Germany, CST STUDIO SUITE v2020. [Online]. Available: https://www.3ds.com/products-services/simulia/products/cst-studio-suite/

[17] Zurich Med Tech, Switzerland, Sim4Life V6.2.1. 2020. [Online]. Available: https://zmt.swiss/sim4life/

[18] P. F. Millington and R. Wilkinson, *Skin*. Cambridge: Cambridge Univ. Press, 1983, pp. 48–51.

[19] International organization for standardization, "Assessment of the safety of magnetic resonance imaging for patients with an active implantable medical device," 2018. [Online]. Available: https://www.iso.org/standard/65055.html

[20] L. Alon, D. K. Sodickson, and C. M. Deniz, "Heat equation inversion framework for average SAR calculation from magnetic resonance thermal imaging," *Bioelectromagnetics*, vol. 37, no. 7, pp. 493–503, 2016.

[21] "GTX medical - restoring the ability to walk by stimulating the spinal cord." [Online]. Available: https://www.gtxmedical.com/

[22] M. Capogrosso *et al.*, "A brain-spine interface alleviating gait deficits after spinal cord injury in primates," *Nature*, vol. 539, no. 7628, pp. 284–288, 2016.

[23] International organization for standardization, "Implants for surgery - active implantable medical devices - Part 3: Implantable neurostimulators," 2017. [Online]. Available: https://www.iso.org/standard/60539.html

[24] G. C. van Rhoon *et al.*, "CEM43°C thermal dose thresholds: A potential guide for magnetic resonance radiofrequency exposure levels?," *Eur. Radiol.*, vol. 23, no. 23, pp. 2215–2227, 2013.

[25] ViP Virtual Population, Accessed on: Jun. 15, 2020. [Online]. Available: https://itis.swiss/virtual-population/virtual-population/vip3/